

# Heterogeneous photocatalyzed oxidation of creosote components: mineralization of xylenols by illuminated TiO<sub>2</sub> in oxygenated aqueous media

Rita Terzian, Nick Serpone \*

Laboratory of Pure and Applied Studies in Catalysis, Environment and Materials, Department of Chemistry, Concordia University, Montreal, Que. H3G 1M8, Canada

Received 7 September 1994; accepted 6 December 1994

## Abstract

Dimethylphenols (xylenols) represent an important component of the phenolic substances in coal tar creosote, a mixture used widely as a wood preservative. The photocatalyzed degradation of all six isomeric forms of xyleneol and the mineralization of 3,4-dimethylphenol were examined in air-equilibrated and oxygenated, illuminated titania dispersions. Some of the hydroxylated intermediates were identified by high performance liquid chromatography (HPLC). The effects of varying the pH, concentration of TiO<sub>2</sub> and xyleneol, temperature and light intensity on the process kinetics were also examined. Kinetic considerations emphasize the notion that the oxidative mineralization process follows natural saturation-type kinetics for which the Langmuir–Hinshelwood model, often invoked in photocatalysis, is a special case; however, it is emphasized that this model is not an a priori requirement in heterogeneous photocatalysis.

*Keywords:* Heterogeneous photocatalysis; Creosote; Xylenols; Titania; Dimethylphenols; Photo-oxidations; Photocatalyzed oxidations

## 1. Introduction

Phenols figure prominently in the list of priority pollutants of the US Environmental Protection Agency [1]. Phenolic substrates, such as xylenols (dimethylphenols), are used as wood preservatives, most notably found as components of coal tar creosote [2]. Together, the six xyleneol isomers comprise about 35 wt.% of the phenolic components. Decontamination of creosote-contaminated sites presents a significant challenge to environmental chemists because of the persistent environmental health risks [2,3]. A comprehensive review of the photo-oxidation of a variety of organics and the relevant underlying principles have recently appeared [4].

The photocatalyzed destruction (mineralization) of the related methylphenols (cresols) has been demonstrated using TiO<sub>2</sub> (Degussa P-25) irradiated by UV-visible light or simulated sunlight [5]; total mineralization was ascertained by the temporal evolution of CO<sub>2</sub>, together with the concomitant disappearance of the original substrate(s).

The work reported here is part of a systematic kinetic and mechanistic study on TiO<sub>2</sub>-mediated photo-oxidations of alkylated phenols. The effects of parameters, such as the pH, initial xyleneol concentration, catalyst loading, radiant power levels of the light source and temperature, were also examined. The primary hydroxylated aromatic intermediates formed during the oxidative process were identified and the rate data were examined in the context of the kinetic principles described earlier [4]. Photochemical efficiencies at 365 nm for the disappearance of the xylenols were also determined.

## 2. Experimental section

### 2.1. Chemicals

2,3-Xyleneol (99%), 2,4-xyleneol (97%), 2,5-xyleneol (better than 99%), 2,6-xyleneol (better than 99.8%), 3,4-xyleneol (99%) and 3,5-xyleneol (better than 99%) were purchased from Aldrich and were used as received. Titanium dioxide was Degussa P-25 (Bru-

\* Corresponding author.

nauer–Emmett–Teller (BET) surface area,  $55 \text{ m}^2 \text{ g}^{-1}$ ; mostly anatase (approximately 80% anatase, 20% rutile) consisting [6] of 99.5%  $\text{TiO}_2$ , <0.3%  $\text{Al}_2\text{O}_3$ , <0.3%  $\text{HCl}$ , <0.2%  $\text{SiO}_2$  and <0.01%  $\text{Fe}_2\text{O}_3$ .

Doubly distilled water was used throughout, unless noted otherwise. The mobile phase used for high performance liquid chromatography (HPLC) analysis consisted of a 50 : 50 mixture of methanol (BDH, Omnisolv grade) and water.

## 2.2. Procedures

Unless otherwise noted, UV–visible irradiation was carried out on aerated, efficiently stirred 50 ml samples. The appropriate quantity of a stock solution of xyleneol was added to a previously weighed amount of  $\text{TiO}_2$  powder to give the required concentration of  $2 \text{ g l}^{-1}$   $\text{TiO}_2$ . The pH was adjusted with  $\text{HCl}$  or  $\text{NaOH}$  as required. Aliquots were taken at various time intervals, filtered to remove suspended particles of  $\text{TiO}_2$  and then analyzed by liquid chromatography (HPLC) [5].

Where  $\text{CO}_2$  evolution was monitored, 25 ml solutions were used; the flasks were sealed with rubber septa and aluminum seals. For experiments in an oxygen atmosphere, the samples were purged for about 15 min with oxygen prior to irradiation. Samples of gas were taken from the headspace volume of the reactor at various time intervals and analyzed by gas chromatography (see below).

For one of the xyleneols, the degradation was also carried out in an oxygen-saturated atmosphere; the flask was oxygen purged for about 10 min. Typically, the temporal course of the mineralization was sampled at approximately 5 min intervals. The flask was removed from the irradiation source, and a suitable aliquot (approximately 2 ml) was taken; subsequently, the flask was again purged with oxygen for 5 min followed by continued irradiation.

Typically, two control runs were carried out for the degradation for each set of experiments. The first involved monitoring the changes in concentration of an identical solution to that being irradiated (i.e. with catalyst present); this solution was stirred in the dark. This was carried out to take into account the thermal component (if any) of the photodegradation reactions. The second experiment involved the irradiation of the dispersion in the absence of catalyst to account for any direct photolysis.

## 2.3. Instrumentation and methodology

The light source used in all the photocatalysis experiments was a 1000 W Hg/Xe lamp operated at about 900 W; it was equipped with a water jacket to filter out IR radiation. The output spectrum (above 220 nm) of the lamp was characterized by strong mercury lines

over the xenon continuum through the visible and UV regions.

The radiant power level dependence of the mineralization process was performed using appropriate neutral density [7] filters in the light path. The radiant power density ( $\text{mW cm}^{-2}$ ) of the light source was obtained with a calibrated power meter (Laser Instrumentation Ltd., model 154BT).

Photochemical efficiencies for the disappearance of xyleneols were determined at 365 nm using a Corning 365 nm interference filter. A specially designed quartz cell having a flat face with a surface area of  $7.07 \text{ cm}^2$  was used. The photochemical efficiencies ( $\xi$ ) [8] were determined according to

$$\xi = \frac{-(dS/dr)}{I_{inc}} \quad (1)$$

where  $-dS/dr$  is the rate of loss of substrate (S) and  $I_{inc}$  is the rate of einsteins of light incident on the exterior walls of the reactor. These efficiencies  $\xi$  will therefore represent lower limits of the true quantum yields ( $\Phi$ ), since estimates are based on the number of photons falling on the external reactor walls and not on the actual number of photons absorbed by the sample. There are inherent difficulties in heterogeneous photocatalysis in determining the amount of light absorbed by the catalysts. Use of the term quantum yield in this context, as described in homogeneous photochemistry and used in heterogeneous photocatalysis, has recently been questioned [8].

The temporal evolution of the mineralization of the various substrates examined in this work and the identification of the reaction intermediates were monitored by HPLC techniques using a Waters Associates liquid chromatograph equipped with a 501 HPLC pump, a 441 absorbance detector, a Rheodyne  $20 \mu\text{l}$  sample injection loop together with a Hewlett-Packard 3396A integrator. The detection wavelengths were 214 nm (Zn lamp), 254 nm and 280 nm (Hg lamp). The column was a Waters reverse phase C-18 ( $\mu$ -Bondapak). All samples were filtered through MSI nylon 66 filters (pore size,  $0.22 \mu\text{m}$ ) prior to analysis.

Carbon dioxide evolution was monitored by gas chromatographic methods using a GOW-MAC gas chromatograph equipped with a Porapak-N (molecular sieve) column and a thermal conductivity detector. Helium was the carrier gas. The instrument was calibrated by either of the following two methods.

- (1) A known quantity of  $\text{CO}_2$  was injected into a nitrogen-purged flask containing a 25 ml aqueous slurry at the desired pH (usually pH 3) of  $2 \text{ g l}^{-1}$   $\text{TiO}_2$ . The flask was subsequently irradiated for 30 min to allow its contents to equilibrate, following which the gases in the headspace were sampled and analyzed by gas chromatography.

(2) Known quantities of  $\text{Na}_2\text{CO}_3$  were added to a  $2 \text{ g l}^{-1}$  suspension of  $\text{TiO}_2$  in water; the flask was sealed and an appropriate quantity of  $\text{HCl}$  was added to bring the suspension to  $\text{pH } 3$ . Subsequently, the sample was irradiated for 1 h, following which the gases in the headspace volume were sampled and injected into the chromatograph.

These methods were used throughout; they take into account any  $\text{CO}_2$  that remained in solution and thus was not present in the headspace. The methods also take into account any photoadsorption of  $\text{CO}_2$  on  $\text{TiO}_2$  that may have occurred on irradiation of the samples.

### 3. Results and discussion

#### 3.1. Catalyst loading

The initial rate of degradation of 3,4-xyleneol ( $160 \mu\text{M}$ ; approximately  $20 \text{ mg l}^{-1}$ ) showed little change on varying the concentration of  $\text{TiO}_2$  between  $0.6$  and  $2 \text{ g l}^{-1}$  (see Fig. 1(a)). A catalyst loading of  $2 \text{ g l}^{-1}$  was therefore used throughout. The plot (Fig. 1(a)) of the initial rates ( $R_{\text{in}}$ ) vs. the  $\text{TiO}_2$  concentration shows

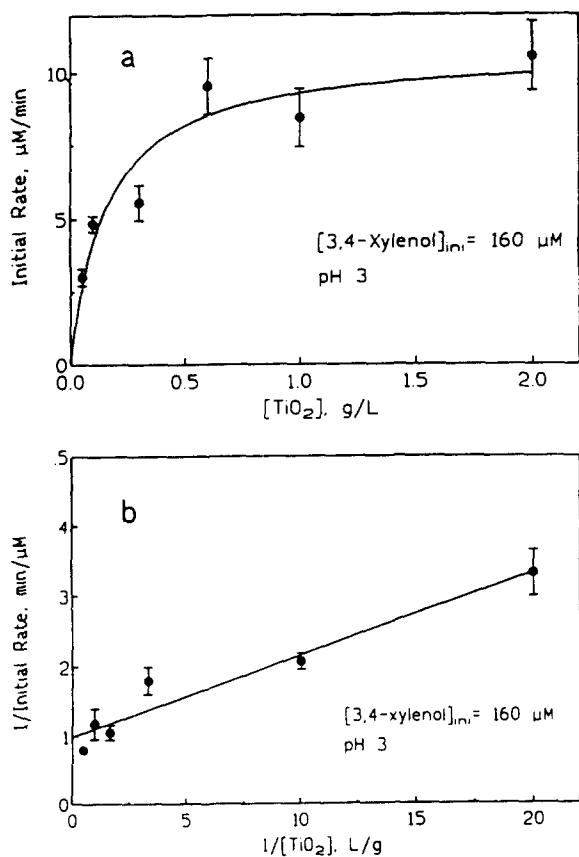
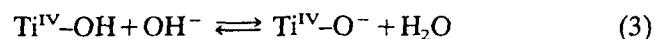
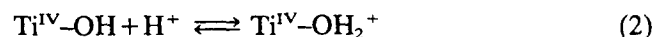


Fig. 1. (a) Plot showing the effect of the  $\text{TiO}_2$  concentration on the initial rate of the photocatalyzed mineralization of  $20 \text{ mg l}^{-1}$  ( $160 \mu\text{M}$ ) of 3,4-xyleneol at  $\text{pH } 3$ . (b) Linear transform of the Langmuir-type expression (see text).

similarities with Langmuir-type behavior:  $R_{\text{in}} = k'_{\text{app}} K_{\text{app}} [\text{TiO}_2] / (1 + K_{\text{app}} [\text{TiO}_2])$  [9]. A computer fit of the data of Fig. 1(a) gave the apparent constant  $k'_{\text{app}} = 13 \pm 2 \mu\text{M min}^{-1}$  and the apparent adsorption coefficient  $K_{\text{app}} = 4 \pm 2 \mu\text{M}^{-1}$ . The linear transform of this expression (Fig. 1(b)) gave  $k'_{\text{app}} = 10 \pm 1 \mu\text{M min}^{-1}$  and  $K_{\text{app}} = 1.2 \pm 0.2 \mu\text{M}^{-1}$ .

#### 3.2. Effect of pH

An important parameter in reactions taking place on semiconductor particulate surfaces is the  $\text{pH}$  of the suspensions, since this dictates the surface charge properties of the photocatalyst. For the  $\text{TiO}_2$  used here, the point of zero charge (pzc) is at  $\text{pH} \approx 5.6$ . Hence, at more acidic  $\text{pH}$  values, the particle surface is positively charged, while at  $\text{pH}$  values above 5.6, it is negatively charged (Eqs. (2) and (3))



This bears significantly on the adsorption-desorption properties of the catalyst's surface, as well as on the photoadsorption-photodesorption features of such surfaces.

Fig. 2 illustrates the effect of  $\text{pH}$  on the rate of photodegradation of 3,4-xyleneol ( $160 \mu\text{M}$ ) in the  $\text{pH}$  range 3–13. Three distinct regions are evident. The first region ( $\text{pH } 3\text{--}5$ ) shows a slight increase in the apparent first-order rate constant ( $k_{\text{app}}$ ) as a function of  $\text{pH}$ ; the second region ( $\text{pH } 5\text{--}10$ ) is relatively uninfluenced by the  $\text{pH}$ ; the third region ( $\text{pH } 10\text{--}13$ ) shows a sharp increase in  $k_{\text{app}}$  as a function of  $\text{pH}$ . Degradation is faster in alkaline media where 3,4-

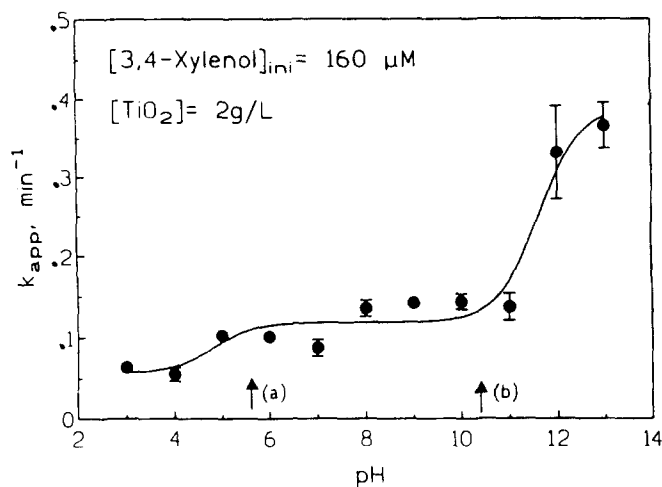


Fig. 2. Plots of the apparent first-order rate constants for the photodegradation of 3,4-xyleneol as a function of initial  $\text{pH}$ . Point (a) indicates the pzc value (approximately 5.6) of the  $\text{TiO}_2$  material used in this work and point (b) indicates the  $\text{pK}_a$  value (10.4) of 3,4-xyleneol.

xylolol is present as the phenoxide species ( $pK_a$  of 3,4-xylolol is 10.4 [10]) and slowest at pH 3.

The slight increase in the rate between pH 3 and 5 and its relative independence of the pH in the range  $5 < \text{pH} < 10$  can best be explained by the charge on the  $\text{TiO}_2$  particle surface. When the surface is positively charged and the phenol is neutral, adsorption probably involves electrostatic attractions between the phenol dipole and the surface charge. Adsorption is diminished when the surface charge is negative. Interactions between the negatively charged  $\text{TiO}_2$  surface and 3,4-xylolol at pH values greater than the  $pK_a$  value are probably stronger as the phenoxide ion is a fairly good nucleophile.

Although alkaline media may seem more suitable to examine the photomineralization of xylolols, we chose to investigate the process details in acidic media (pH 3) to avoid possible direct photolysis of the xylolols, as witnessed in earlier studies on the photocatalyzed mineralization of 4-chlorophenol [11] and pentachlorophenol [12].

### 3.3. Identification of intermediates

High performance liquid chromatograms revealed that eight (1–8) detectable intermediates were formed for the six xylolols surveyed. A comparison of the retention times aided considerably in the identification of these intermediates with specific species formed by monohydroxylation. In addition, dihydroxybenzenes have a relatively large absorbance at  $\lambda = 214$  nm ( $\log \epsilon \approx 3.8$ ) and a small absorbance at  $\lambda = 254$  nm, whereas benzoquinones have high extinction coefficients at 254 nm ( $\log \epsilon \approx 4.3$ ) and absorb little at 214 nm. Where possible, the nature of the species formed on reaction of  $\cdot\text{OH}$  radicals with xylolols (dihydroxydimethylbenzenes and dimethylbenzoquinones) was confirmed from commercially available pure substrates run under otherwise identical conditions. (The retention time (HPLC) of 2,3-dimethylbenzoquinone was obtained by synthesizing it via oxidation of an aqueous solution of 2,3-dimethylhydroquinone by bubbling air overnight.)

Photo-oxidation of 2,3-xylolol yields three intermediates: 2,3-dimethylbenzoquinone (3) and trace quantities of intermediates 1 and 2 (Table 1). The latter is 2,3-dimethylhydroquinone, while species 1, also detected in the photo-oxidation of 3,4-xylolol, is inferred to be 3,4-dimethylcatechol. The photo-oxidation of 2,4-xylolol produced no HPLC-detectable intermediates under our experimental conditions. By contrast, 2,5-xylolol gave 2,5-dimethylbenzoquinone (2,5-DMBQ; 4).

Two intermediates were detected in the photodegradation of 2,6-xylolol (5 and 6). Species 6 is 2,6-dimethylbenzoquinone (2,6-DMBQ), while species 5, detected in trace amounts, is probably 2,6-dimethyl-

hydroquinone (2,6-DMHQ); it was also detected in the mineralization of 3,5-xylolol. A single intermediate (1) was detected in the photodegradation of 3,4-xylolol: it is 3,4-dimethylcatechol (3,4-DMCC), also formed in the photodegradation of 2,3-xylolol. Finally, four intermediates were detected in the photodegradation of 3,5-xylolol, three (5, 7 and 8) in trace quantities. The major intermediate 6 is 2,6-DMBQ, while intermediate 5, also detected in the photo-oxidation of 2,6-xylolol, is inferred to be 2,6-DMHQ. The nature of species 7 and 8 remains enigmatic; a possibility is 3,5-dimethylcatechol (3,5-DMCC), also expected, but not detected, in the photomineralization of 3,5-xylolol. It is possible that the quantity of 3,5-DMCC was too small to be detected under our conditions. In addition, trihydroxydimethylbenzenes are not precluded for either 7 or 8 since trihydroxylated benzenes have been reported in the photomineralization of phenol, albeit in trace quantities: 0.3% pyrogallol and 2.1% hydroxyhydroquinone [13].

Other intermediate products that could form in these methylated phenols are those resulting from hydrogen abstraction by  $\cdot\text{OH}$  radicals, known to react with methylbenzenes (e.g. toluene and xylenes) in homogeneous solution [14], but at slower rates (by about two orders of magnitude) than  $\cdot\text{OH}$  adduct formation. The nature of intermediates 1–8 is summarized in Table 1.

### 3.4. Rate data for the degradation of xylolols

None of the xylolols investigated in this work undergo detectable changes in the dark in the presence of  $\text{TiO}_2$ . Therefore degradation originates with light-induced processes. Direct photolysis of aqueous xylolol solutions led to very small decreases in xylolol concentration (less than 5% after approximately 1 h). For 20 mg  $\text{l}^{-1}$  of the xylolols, the apparent rate constants are  $(2.9 \pm 0.7) \times 10^{-4} \text{ min}^{-1}$  (2,3-xylolol),  $(11 \pm 1) \times 10^{-4} \text{ min}^{-1}$  (2,4-xylolol),  $(7 \pm 2) \times 10^{-4} \text{ min}^{-1}$  (2,5-xylolol),  $(7.5 \pm 0.6) \times 10^{-4} \text{ min}^{-1}$  (2,6-xylolol),  $(19 \pm 1) \times 10^{-4} \text{ min}^{-1}$  (3,4-xylolol) and  $(7.4 \pm 0.5) \times 10^{-4} \text{ min}^{-1}$  (3,5-xylolol). The rate constants for direct photolysis are about one or two orders of magnitude smaller than those for catalyzed processes ( $5.4 \times 10^{-2}$ – $12 \times 10^{-2} \text{ min}^{-1}$ ; see Table 2).

The photocatalyzed decomposition of the six xylolols in the presence of  $\text{TiO}_2$  is presented in Figs. 3(a)–3(f). All six xylolols (20 mg  $\text{l}^{-1}$ ) degrade via first-order kinetics under otherwise identical conditions of light source, initial pH and  $\text{TiO}_2$  concentration. The formation and subsequent degradation of the major intermediates detected in each case are also indicated. In every instance, total disappearance of the original xylolol and decomposition of the intermediate species occur in less than 1 h of irradiation. The corresponding

Table 1  
Intermediates identified during the course of the mineralization of xylenols

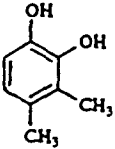
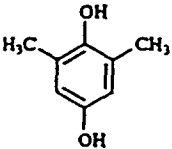
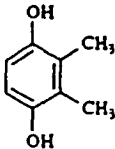
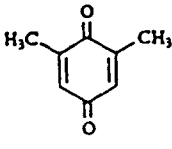
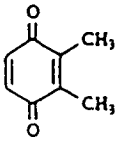
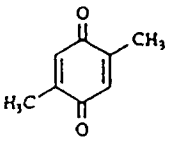
Intermediate	Identification	Intermediate	Identification
1	 3,4-Dimethylcatechol	5	 2,6-Dimethylhydroquinone
2	 2,3-Dimethylhydroquinone	6	 2,6-Dimethylbenzoquinone
3	 2,3-Dimethylbenzoquinone	7	See text
4	 2,5-Dimethylbenzoquinone	8	See text

Table 2  
Apparent kinetics of mineralization of xylenols photocatalyzed by irradiated TiO<sub>2</sub> in air-equilibrated suspensions at pH 3

Xylenol	[Xylenol] ( $\mu\text{M}$ )	$k_{\text{app}}$ ( $10^{-2} \text{ min}^{-1}$ )	Initial rate ( $\mu\text{M min}^{-1}$ )	$t_{1/2(\text{app})}$ (min)
2,3-Xylenol	168.0	$7.9 \pm 0.5$	$13.4 \pm 0.9$	8.7
	162.0	$6.3 \pm 0.9$	$10.1 \pm 1.5$	11.1
2,4-Xylenol	165.5	$11 \pm 1$	$18 \pm 2$	6.3
	177.7	$9.1 \pm 0.7$	$16 \pm 1$	7.6
2,5-Xylenol	156.7	$7.6 \pm 0.4$	$11.8 \pm 0.7$	9.2
	163.2	$7.5 \pm 0.4$	$12.2 \pm 0.7$	9.2
2,6-Xylenol	163.3	$11.3 \pm 0.6$	$19 \pm 1$	6.1
	164.2	$12.0 \pm 0.8$	$20 \pm 1$	5.8
3,4-Xylenol	16.3	$28 \pm 4$	$4.6 \pm 0.7$	2.5
	41.8	$17 \pm 1$	$7.2 \pm 0.5$	4.0
	85.8	$10 \pm 1$	$8.6 \pm 1.0$	6.9
	158.1	$8.5 \pm 0.6$	$13.5 \pm 0.9$	8.1
	158.4	$7.9 \pm 0.4$	$12.4 \pm 0.7$	9.8
	156.3	$6.4 \pm 0.4$	$10.0 \pm 0.6$	10.9
	164.2	$7 \pm 1$	$12 \pm 2$	9.9
	407.2	$3.9 \pm 0.3$	$16 \pm 1$	17.9
3,5-Xylenol	166.3	$6.4 \pm 0.5$	$10.7 \pm 0.8$	10.8
	165.3	$5.4 \pm 0.3$	$8.9 \pm 0.5$	12.9

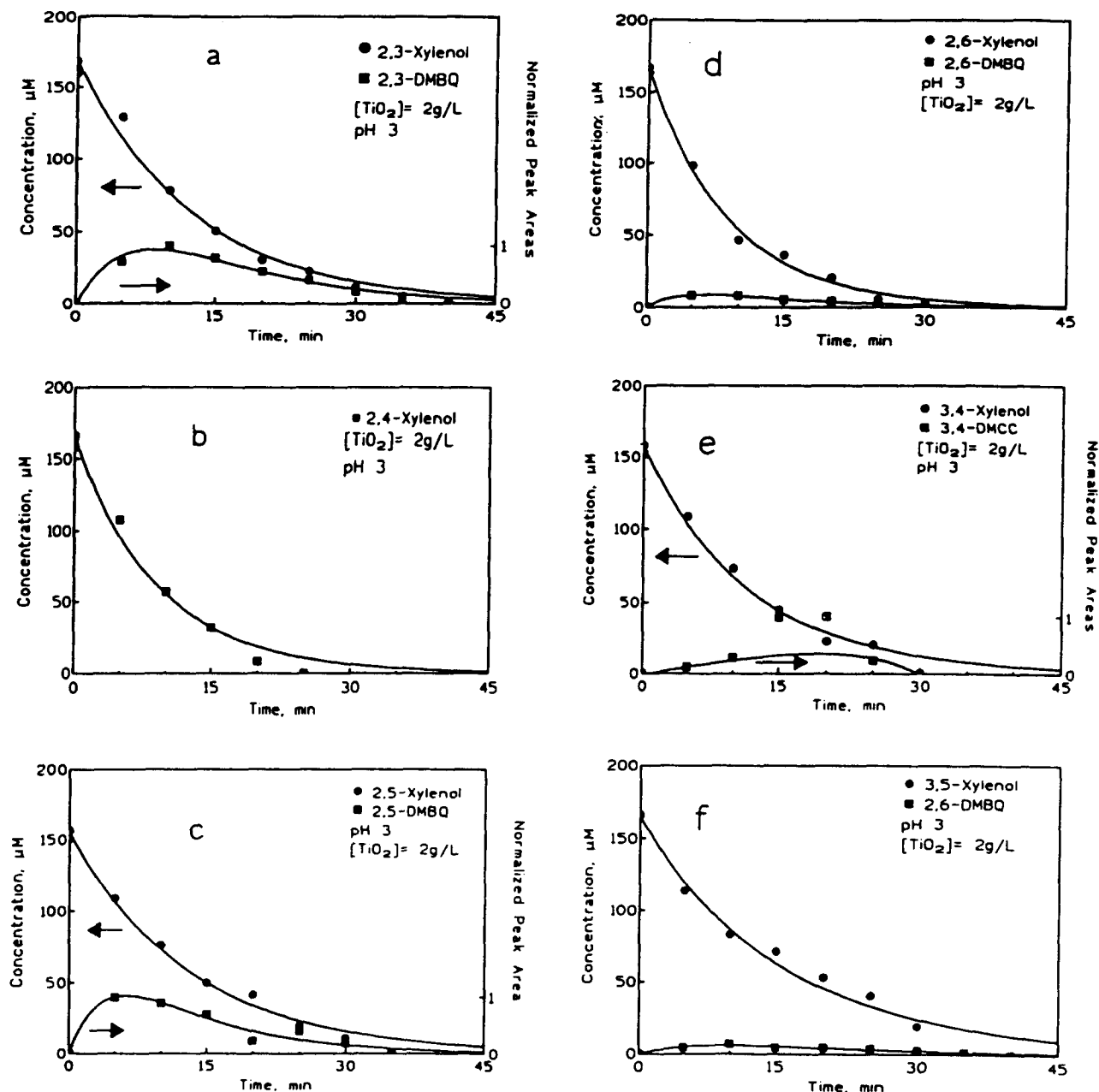
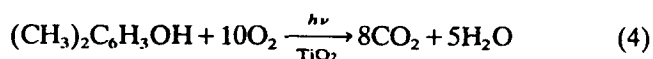


Fig. 3. Plots of the normalized peak areas (or concentration) as a function of irradiation time showing the degradation of the six xylenols (approximately  $20 \text{ mg l}^{-1}$ ) and the formation and decomposition of the major intermediates in the photomineralization process with irradiated  $\text{TiO}_2$  present ( $2 \text{ g l}^{-1}$  at pH 3): (a) 2,3-xylenol; (b) 2,4-xylenol; (c) 2,5-xylenol; (d) 2,6-xylenol; (e) 3,4-xylenol; (f) 3,5-xylenol. The curves are computer fits to the equations noted in the text.

apparent rate constants, initial rates and half-lives for the degradation of the six xylenols as a function of the initial concentration are summarized in Table 2.

The apparent kinetic parameters for the formation and subsequent degradation of the major intermediates produced during the course of mineralization of the six xylenols are presented in Table 3. All the intermediates are formed and decay via apparent first-order kinetics, except for 3,4-DMCC observed during the photodegradation of 3,4-xylenol; it is formed via first-order processes, but disappears via zero-order kinetics.

The photocatalyzed mineralization process for the six xylenols follows the stoichiometric reaction (4), demonstrated by a quantitative product analysis in the case of 3,4-xylenol



The temporal evolution of  $\text{CO}_2$  is illustrated in Fig. 4 for an  $\text{O}_2$ -saturated aqueous solution of 3,4-xylenol. Approximately  $33 \mu\text{mol}$  of  $\text{CO}_2$  is expected from reaction (4) for  $[\text{3,4-xylenol}]_{\text{ini}} = 165 \mu\text{M}$ . Evidently, after about

Table 3

Apparent kinetics of formation of intermediates produced at pH 3 in air-equilibrated, irradiated TiO<sub>2</sub> suspensions

Parameter	Source					
	2,3-Xylenol	2,4-Xylenol	2,5-Xylenol	2,6-Xylenol	3,4-Xylenol	3,5-Xylenol
[Xylenol] ( $\mu\text{M}$ )	168.3	165.5	156.7	163.3	158.1	166.32
$k_{\text{app}}$ (degradation) ( $\text{min}^{-1}$ )	0.079	0.11	0.076	0.11	0.085	0.064
$k_{\text{app}}$ (formation) ( $\text{min}^{-1}$ )						
2,3-Dimethylbenzoquinone	0.12	–	–	–	–	–
2,5-Dimethylbenzoquinone	–	–	0.10	–	–	–
2,6-Dimethylbenzoquinone	–	–	–	0.093	–	0.090
3,4-Dimethylcatechol	–	–	–	–	0.085	–
$k_{\text{app}}$ (degradation) ( $\text{min}^{-1}$ )						
2,3-Dimethylbenzoquinone	0.12	–	–	–	–	–
2,5-Dimethylbenzoquinone	–	–	0.24	–	–	–
2,6-Dimethylbenzoquinone	–	–	–	0.24	–	0.12
3,4-Dimethylcatechol ( $\mu\text{M min}^{-1}$ )	–	–	–	–	0.32	–

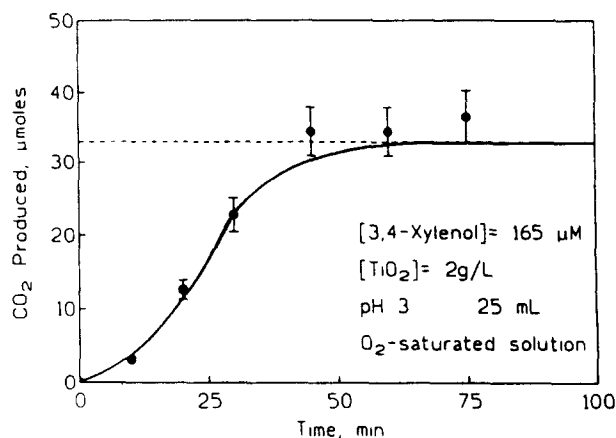


Fig. 4. Plot showing the temporal evolution of CO<sub>2</sub> from the photomineralization of 165  $\mu\text{M}$  xylenol in the presence of 2 g l<sup>-1</sup> TiO<sub>2</sub> at an initial pH of 3 in an oxygen-saturated suspension.

1 h of irradiation, when all the xylenol and the aromatic intermediate species had decomposed, the expected stoichiometric amount of CO<sub>2</sub> was reached in less than about 45 min.

### 3.5. Effect of oxygen

The effect of varying the concentration of molecular O<sub>2</sub> on the kinetics of decomposition of 3,4-xylenol was assessed by examining the photoreaction under conditions in which the suspension was saturated with O<sub>2</sub>. The decomposition of this xylenol in both air-equilibrated and O<sub>2</sub>-saturated suspensions is compared in Fig. 5. Good first-order kinetics are evident in both cases. The corresponding parameters are (air vs. O<sub>2</sub>):  $k_{\text{app}}$ , 0.085 min<sup>-1</sup> vs. 0.16 min<sup>-1</sup>; initial rates, 13.5  $\mu\text{M min}^{-1}$  vs. 27.1  $\mu\text{M min}^{-1}$ ;  $t_{1/2}(\text{app})$ , 8.1 min vs. 4.3 min. In the presence of excess oxygen, the conversion of 3,4-xylenol occurred in less than about 15 min.

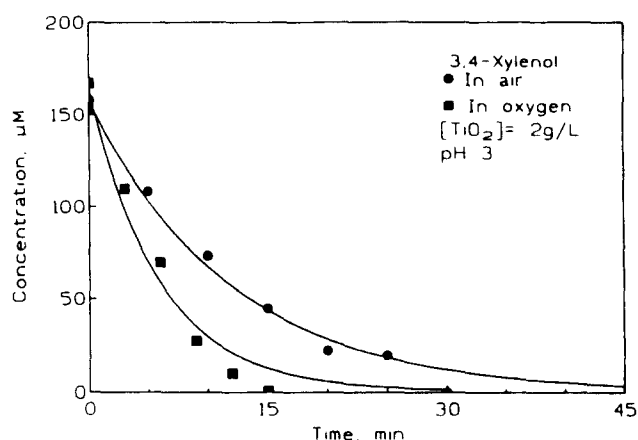


Fig. 5. Plot showing the photodegradation of approximately 20  $\mu\text{M}$  of 3,4-xylenol in the presence of 2 g l<sup>-1</sup> TiO<sub>2</sub> in air-equilibrated suspensions and oxygen-saturated suspensions; initial pH 3. The apparent rate constants  $k_{\text{app}}$  were (air vs. O<sub>2</sub>): 0.085 min<sup>-1</sup> vs. 0.16 min<sup>-1</sup>.

### 3.6. Concentration dependence

The photomineralization of 3,4-xylenol occurs via first-order kinetics at all the concentrations examined (16.3  $\mu\text{M}$  (approximately 2 mg l<sup>-1</sup>) to 407.2  $\mu\text{M}$  (approximately 50 mg l<sup>-1</sup>)). The initial rates (Fig. 6 and Table 2) vary from 4.6  $\mu\text{M min}^{-1}$  to 16  $\mu\text{M min}^{-1}$ . A plot of the initial rates ( $R_{\text{in}}$ ) vs. initial [3,4-xylenol] shows saturation-type kinetic behavior (Fig. 7(a)):  $R_{\text{in}} = k'_{\text{app}} K_{\text{app}} [3,4\text{-xylenol}] / (1 + K_{\text{app}} [3,4\text{-xylenol}])$  [9]. A computer fit of the data of Fig. 7(a) to this Langmuir-like expression gave  $k'_{\text{app}} = 18 \pm 2 \mu\text{M min}^{-1}$  and  $K_{\text{app}} = 0.014 \pm 0.004 \mu\text{M}^{-1}$ . The linear transform of this expression (Fig. 7(b)) gave  $k'_{\text{app}} = 14 \pm 2 \mu\text{M min}^{-1}$  and  $K_{\text{app}} = 0.030 \pm 0.004 \mu\text{M}^{-1}$ .

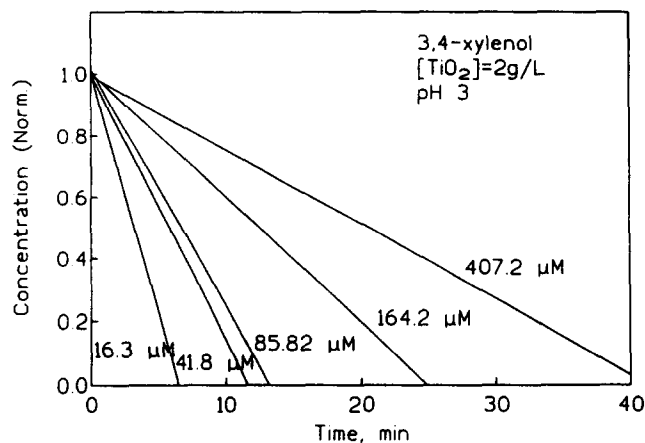


Fig. 6. Plot showing the initial rates of photomineralization of 3,4-xyleneol catalyzed by irradiated  $\text{TiO}_2$  at various initial concentrations; initial pH 3.

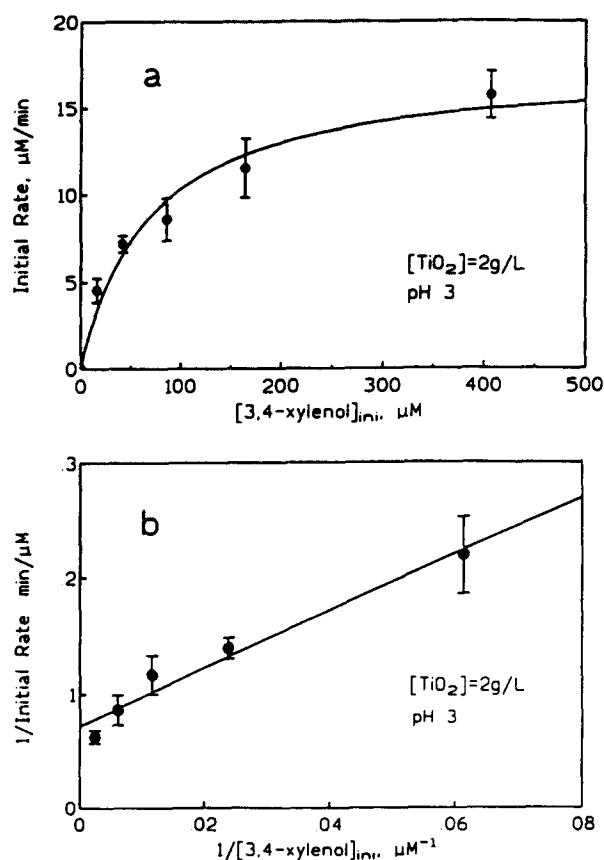


Fig. 7. (a) Plot showing the effect of the initial concentration on the initial rate of photodegradation of 3,4-xyleneol under air-equilibrated conditions; initial pH 3. (b) Linear transform of the Langmuir-type expression (see text).

### 3.7. Radiant power level dependence

The effect of the light intensity on the rate of photo-oxidation was recently examined using simple considerations and assumptions [15,16]: (a) a steady state exists for reactive species; (b) the photocatalyst surface is rapidly and completely hydroxylated; (c) degradation

implicates  $\cdot\text{OH}$  radicals; (d) the number of photogenerated electrons equals the number of photoproduced holes; (e) recombination involves electron-hole pairs; (f) there is rapid mass transfer of the substrate onto the photocatalyst surface. The rate of destruction of a pollutant substrate  $S$  is  $r_s = k[\cdot\text{OH}][S]$ , which under steady state conditions for the production of  $\cdot\text{OH}$  radicals converts to

$$r_s = k \frac{k_{\text{H}_2\text{O}}[h^+][\text{H}_2\text{O}]}{k_{\text{OH}} + k[S] + \sum k_{\text{intm}}[\text{intm}]} [S] \quad (5)$$

For steady state conditions in the formation of holes ( $[h^+] = [e^-]$ ) and at relatively high intensities (high  $[h^+]$ ), electron-hole pair recombination predominates over  $h^+$  trapping by surface-bound  $\text{OH}^-$  and/or  $\text{H}_2\text{O}$  and yields [15]

$$[h^+] = \sqrt{\frac{k_{\text{exc}}I}{k_{\text{rec}}}} \quad (6)$$

Thus  $r_s$  varies with  $I^{1/2}$ . At low light intensities,  $h^+$  trapping competes effectively with  $e^- - h^+$  recombination to give

$$[h^+] = \frac{k_{\text{exc}}I + k_{\text{OH}}[\cdot\text{OH}]}{k_{\text{H}_2\text{O}}[\text{H}_2\text{O}]} \quad (7)$$

where  $r_s$  scales with  $I$ . Similar conclusions have been reached by Peterson et al. [17].

At high intensities, the expected rate-limiting factor is mass transfer, i.e. the rate of photodegradation becomes independent of  $I$  ( $r_s$  scales with  $I^0$ ) [18].

The results reported here are in accord with the above expectations. It is evident from these and other results that it is more advantageous to work at low light fluxes.

The dependence of the rate of photodegradation of 3,4-xyleneol (165  $\mu\text{M}$ ) on the radiant power level of the light source is illustrated in Fig. 8(a). The plot comprises three distinct regimes: A, B and C. In regime A (Fig. 8(b)), the rate increases linearly with the power level (low light fluxes). In regime B, the rate increases as the square root of the power level (see Fig. 8(c)). Finally, in regime C (Fig. 8(b)), the rate is independent of the power density. The direct dependence of the rate on the radiant power at low densities ( $I \leq 12\%$ ) and on its square root at higher densities ( $19.1\% \leq I \leq 65.8\%$ ) is similar to the behavior noted by others for the photo-oxidation of isopropanol [16], phenol [13] and 3-chlorophenol [19].

### 3.8. Photochemical efficiencies

Because the band gap of  $\text{TiO}_2$  is 3.2 eV, only light wavelengths lower than 400 nm can drive a titania-assisted photocatalytic process. The photochemical efficiencies were determined at 365 nm. It must be



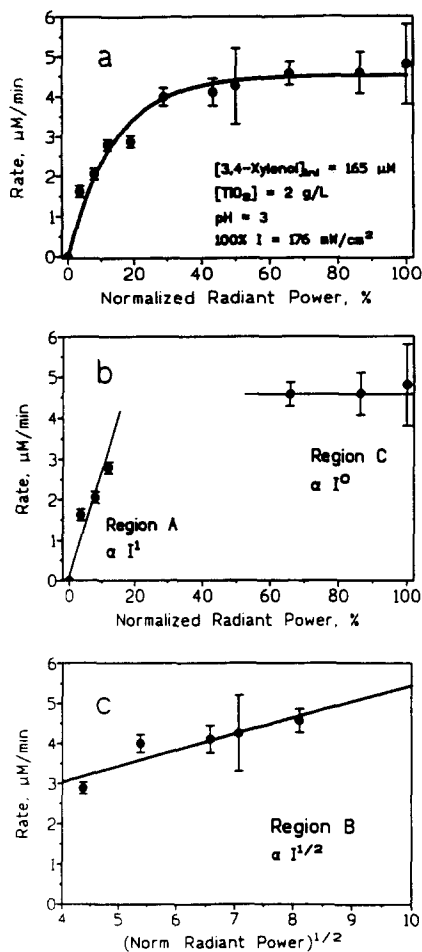


Fig. 8. (a) Effect of the radiant power levels of the light source (see text) on the initial rate of photomineralization of 3,4-xyleneol (165  $\mu\text{M}$ ); initial pH 3;  $\text{TiO}_2$ , 2  $\text{g l}^{-1}$ ; 100% radiant power corresponds to 176  $\text{mW cm}^{-2}$ . (b) Regions where the dependence of the initial rate on the radiant power level is a function of  $I^1$  at low light fluxes and  $I^0$  at high light fluxes. (c) Region where the initial rate is a function of the square root of the radiant power at intermediate light fluxes.

emphasized that they reflect the number of molecules of xyleneol that degrade per photon incident on the external reactor walls (see Section 2.3). The efficiencies  $\xi$  are 0.0060 (3,4-xyleneol), 0.0067 (2,3-xyleneol), 0.0067 (3,5-xyleneol), 0.0074 (2,5-xyleneol), 0.012 (2,4-xyleneol) and 0.015 (2,6-xyleneol). These results are comparable with those reported earlier [5] for cresol under otherwise identical conditions (0.0096 (*o*-cresol), 0.0076 (*m*-cresol) and 0.010 (*p*-cresol)). Moreover, it is noteworthy that these lower limits of the true quantum yields ( $\Phi$ ) are in keeping with a recent assessment of the quantum yield of formation of  $\cdot\text{OH}$  radicals, the major oxidizing entity, of approximately 0.04 [20] and with our own assessment that  $\Phi$  must be less than 0.10 [21].

### 3.9. Effect of Degussa P25 $\text{TiO}_2$ batch variation

The origin and/or method of preparation of  $\text{TiO}_2$  particulates has a significant influence on the photo-

catalytic properties and therefore the process [22]. For the  $\text{TiO}_2$  used here, we examined the effect(s) of varying the batch of material by probing the degradation of 3,4-xyleneol using three different batches of Degussa P25  $\text{TiO}_2$ . The results are shown in Fig. 9 and the kinetic parameters are summarized in Table 4.

The slight variations in the kinetic parameters for different batches of Degussa  $\text{TiO}_2$  are similar to those observed for different runs using the same batch of  $\text{TiO}_2$  (see Table 2). Thus changing the batch of Degussa  $\text{TiO}_2$  had no significant effect on the rate of photodegradation of 3,4-xyleneol.

### 3.10. Initial mechanistic route in the photodegradation of xyleneols

Photo-oxidations occur by reaction between surface-bound  $\cdot\text{OH}$  radicals (or equivalent surface oxidizing species) and the various xyleneols as a first step; this yields the intermediates noted earlier, namely 2,3-DMBQ, 2,5-DMBQ, 2,6-DMBQ, 3,4-DMCC and others. Further reaction of these intermediates with  $\cdot\text{OH}$  species ultimately yields  $\text{CO}_2$  (and  $\text{H}_2\text{O}$ ) via a complex series of reactions, which include ring cleavage and the formation of peroxides, aldehydes and carboxylates [23]. The initial steps of the photomineralization process are summarized in Eq. (8). The ring-cleaved products tend

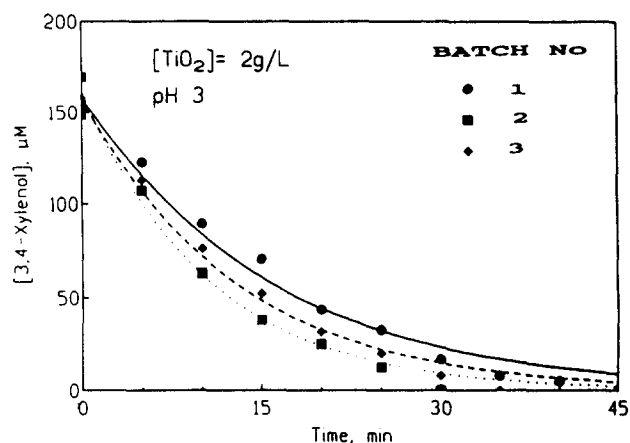


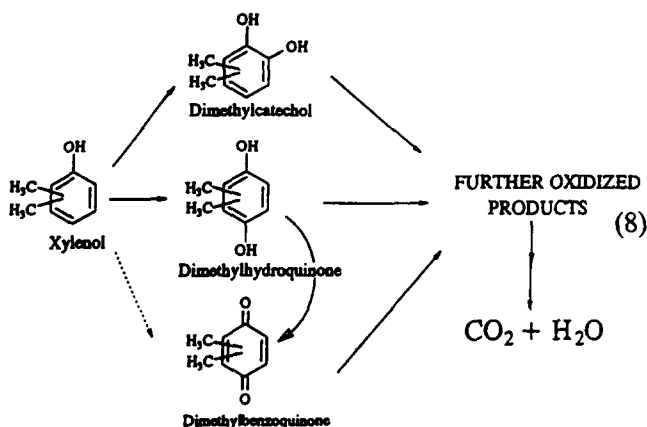
Fig. 9. Plot showing the effect of different batches of Degussa P25  $\text{TiO}_2$  on the rate of photodegradation of 3,4-xyleneol;  $[\text{3,4-xyleneol}]_{\text{ini}} = 160 \mu\text{M}$ ; pH 3;  $[\text{TiO}_2] = 2 \text{ g l}^{-1}$ .

Table 4

Kinetic parameters for the disappearance of 3,4-xyleneol obtained in the  $\text{TiO}_2$  batch dependence study;  $[\text{3,4-xyleneol}] = 160 \mu\text{M}$ ,  $[\text{TiO}_2]$  (Degussa P25) = 2  $\text{g l}^{-1}$ , pH 3

Batch	$k_{\text{app}}$ ( $\text{min}^{-1}$ )	Initial rate ( $\mu\text{M min}^{-1}$ )	$t_{1/2}$ (min)
1	$0.064 \pm 0.004$	$10.6 \pm 0.7$	10.9
2	$0.094 \pm 0.007$	$15.5 \pm 1.0$	7.3
3	$0.078 \pm 0.004$	$12.9 \pm 0.7$	8.8

to elude detection (under our conditions) and were not examined further.



### 3.11. Effect of temperature

The effect of temperature on the rate of photodegradation of 3,4-xyleneol was examined in the range 6–60 °C. The results are depicted in Fig. 10(a). The initial rates increase with increasing temperature. The Arrhenius activation energy (Fig. 10(b)) for the reaction is  $E_a = 2.1 \pm 0.2$  kcal mol<sup>-1</sup>, comparable with that reported by Okamoto et al. [13] for the photodegradation of phenol (2.4 kcal mol<sup>-1</sup>) and by Al-Sayed et al. [24] for the degradation of 4-chlorophenol (1.3 kcal mol<sup>-1</sup>). These low values show that thermally activated steps are negligible; adsorption–desorption processes are nearly temperature independent in this range [24]. The enthalpy and entropy of activation were estimated from Eyring plots (Fig. 10(c)):  $\Delta H^\ddagger = 1.4 \pm 0.2$  kcal mol<sup>-1</sup> and  $\Delta S^\ddagger = -50 \pm 10$  cal K<sup>-1</sup> mol<sup>-1</sup>. The large negative  $\Delta S^\ddagger$  value is consistent with a reaction between adsorbed (or photoadsorbed) xyleneol and the surface-bound oxidizing species photogenerated on TiO<sub>2</sub> particles during irradiation.

### 3.12. Kinetic considerations

Describing the kinetics in a heterogeneous photocatalytic system is a challenging task, because of the complex nature of the catalyst's surface, which interacts to different extents with the solvent, initial substrate, intermediate species and any other adventitious impurities present in the dispersion. The picture is further complicated by the effect photons have on the surface properties, such as on the adsorption–desorption equilibria and the nature of the catalytic sites. Until the precise influence of these factors on the photo-oxidative process is understood, the process kinetics in heterogeneous photocatalysis must be considered as apparent kinetics.

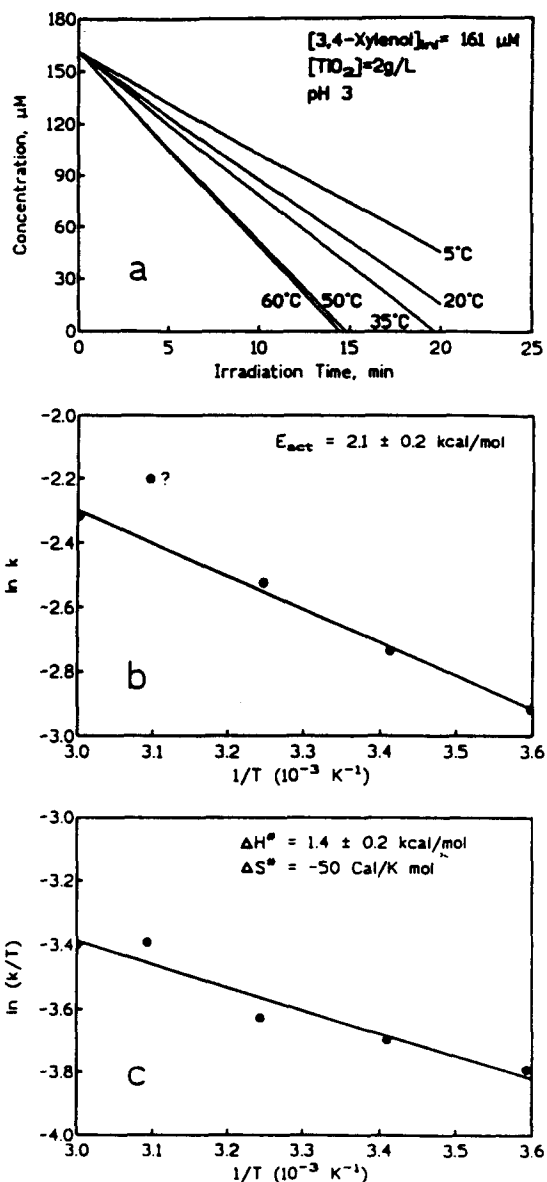
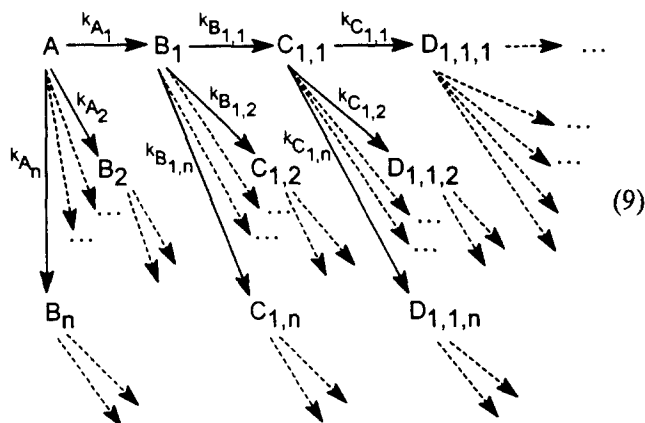


Fig. 10. (a) Temperature dependence of the initial rate of photodegradation of 3,4-xyleneol. (b) Arrhenius ( $\ln k$  vs.  $1/T$ ) plot for the photodegradation of 3,4-xyleneol. (c) Eyring ( $\ln(k/T)$  vs.  $1/T$ ) plot for the photodegradation of 3,4-xyleneol.

The photo-oxidation processes of various phenolic substrates typically proceed via consecutive and parallel stages. The products formed on primary hydroxylation of the substrate are the corresponding catechols, hydroquinones and *p*-benzoquinones. On subsequent  $\cdot\text{OH}$  radical attack, these primary hydroxylation products form species with higher oxygen-to-carbon content. In turn, they may be subjected to further attack by  $\cdot\text{OH}$  radicals, eventually leading to benzene ring opening and to the formation of a series of intermediates of progressively higher oxygen-to-carbon ratios. Ultimately, the species are oxidized quantitatively to carbon dioxide (and H<sub>2</sub>O). The exact number of intermediates and the extent of interaction of each one with the surface of the catalyst remain unknown.

Earlier [24], we modelled the photocatalytic process for the oxidation of various aromatic substrates, on the basis of the above constraints, in the most simplistic form by the consecutive and parallel reactions illustrated in Eq. (9);  $B_i$  and  $C_{ij}$  are the intermediates formed after  $\cdot\text{OH}$  attack on species A and  $B_i$  respectively.

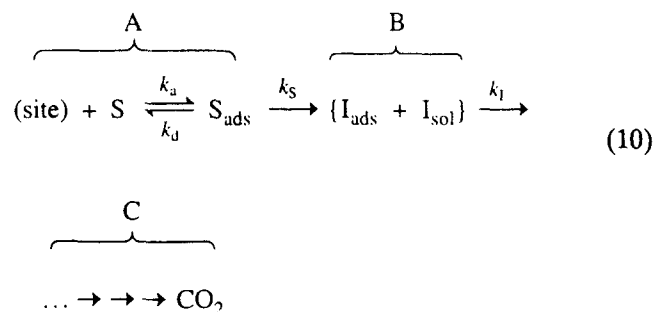


Taking  $k_A$  and  $k_B$  as  $\sum_i k_{A_i}$  and  $\sum_j k_{B_{ij}}$  respectively, the concentrations of A,  $B_i$  and  $C_{ij}$  at some time  $t$  may be obtained for first-order processes by expressions reported elsewhere [5,9]. The formation of  $\text{CO}_2$  followed in nearly all cases simple exponential growth kinetics:  $[\text{CO}_2] = \text{constant}[1 - \exp(-k_p t)]$ .

Assigning an operational mechanism for reactions taking place in heterogeneous media to a Langmuir-type process (i.e. adsorption followed by oxidative attack by active oxygen species as exemplified in gas–solid systems) or to an equivalent type process is not possible on the basis of the observed kinetics alone [15]. Therefore, although the analytical expression obtained for the rate of photo-oxidation is analogous to the Langmuir–Hinshelwood relationship, nothing can be concluded about the operational mechanism in heterogeneous photocatalysis. This point cannot be emphasized enough. Many of the models that follow Langmuir-type behavior are simply various manifestations of saturation-type kinetics that are general in chemical kinetics, even in the homogeneous phase (e.g. in enzymatic reactions).

We suggested earlier [8] that, in heterogeneous photocatalysis involving solution–solid interfaces, the events should be described by a simple model (see below). Most of the evidence generated in various laboratories indicates that many, if not all, of the events are surface-occurring events. The expression(s) describing these will parallel those of saturation-type kinetics. However, no a priori assumptions are made in the model as to the exact nature of the kinetic expressions which define the events. A few additional points should be noted. We begin by recognizing that the extent of photoadsorption is unknown. In developing rate expressions

for the photo-oxidation process, it is implicitly assumed, therefore, that there is a constant fraction, however small, of the organic substrate on the catalyst's oxidative active surface sites. One or more intermediates ( $I_{\text{ads}}$  and/or  $I_{\text{sol}}$ ) form following  $\cdot\text{OH}$  attack on the aromatic ring of the substrates  $S_{\text{ads}}$ . They subsequently or nearly simultaneously undergo fragmentation to aliphatic species, which ultimately also degrade to produce stoichiometric amounts of  $\text{CO}_2$  (Eq. (10))



where  $k_s$  denotes the sum of rate constants for the formation of various intermediate species and  $k_1$  represents the sum of rate constants for the fragmentation of these intermediates. The rate of product formation is then given by [9]

$$\text{Rate} = \frac{k_s K_s N_s [S]}{1 + [(k_s + k_1)/k_1] K_s [S]} \quad (11)$$

where  $K_s (=k_a/(k_d + k_s))$  is the photoadsorption coefficient for the substrate and  $N_s$  is the number of oxidative sites. The similarity of Eq. (11) to the Langmuir–Hinshelwood kinetic rate law should be noted [12]. Considering that  $\cdot\text{OH}$  radicals are formed from a light-assisted process, their formation and disappearance through back reactions also need to be accounted for in the expression for the overall rate of product formation.

The quantum yield of formation of  $\cdot\text{OH}$  species (approximately 4% [20]) is  $\Phi_{\cdot\text{OH}} = \phi I_a^n k_{\text{trap}} \tau$  (at low light fluxes,  $n=1$ ) where  $\tau$  is the lifetime of the valence band holes of the photocatalyst ( $\tau = 1/(k_{\text{rec}} + k_{\text{trap}})$ ) and  $k_{\text{trap}}$  and  $k_{\text{rec}}$  are the rate constants for the formation of trapped holes and the recombination of electron–hole pairs respectively. If  $k_{\text{rec}} > k_{\text{trap}}$  [25], then  $\Phi_{\cdot\text{OH}} = \phi I_a \beta A_p k_{\text{trap}} / k_{\text{rec}}$ , where  $\beta A_p$  denotes the fraction of the particle surface that is irradiated and  $A_p$  is the particle surface area. The overall rate will also depend on the lifetime of the surface-bound  $\cdot\text{OH}$  radicals  $\tau_{\cdot\text{OH}}$ . Various species, such as water, intermediates, ions and other adventitious impurities, can compete with xylene for the same adsorption sites and thus act as inhibitors. The apparent rate of formation of products then becomes

Rate =

$$\frac{[(\phi I_a \beta A_p k_{\text{trap}} \tau_{\text{OH}}) / k_{\text{reco}}] k_s K_s N_s [S]_0}{1 - [(k_s + k_1) / k_1] K_s [S] + K_w [H_2O] + K_I [I] + K_{\text{ions}} [\text{Ions}]}$$

$$\times \frac{K_{O_2} [O_2]}{(1 + K_{O_2} [O_2])} \quad (12)$$

Expression (12) is similar to those proposed by others [13,15], but is more global as it takes into account many of the properties of the systems examined, including the absorption of light by the catalyst, the formation and recombination of electrons and holes in the semiconductor, the formation of the oxidizing species, the lifetime of the active species and the adsorption properties of all the species involved including any intermediates produced.

The Langmuir adsorption isotherm for  $O_2$  is included in Eq. (12) since molecular oxygen has a significant effect on the rate of degradation; it is applicable under conditions of low ( $n=1$ ), medium ( $n=1/2$ ) and high ( $n=0$ ) light fluxes.

#### 4. Conclusions

Transformation of 2,3-, 2,4-, 2,5-, 2,6-, 3,4- and 3,5-xylene in air-equilibrated, irradiated  $TiO_2$  suspensions takes place in less than 1 h at pH 3. In the presence of excess molecular  $O_2$ , the degradation of 3,4-xylene is even faster (15 min or less) and complete mineralization to  $CO_2$  and  $H_2O$  takes place in approximately 1 h. Various experimental factors, such as pH, temperature, photocatalyst concentration, substrate concentration and light flux, influence the overall rate of degradation; they were examined in some detail for 3,4-xylene. The rate of the photocatalyzed reaction increases with pH and temperature. Concentration dependence experiments (varying  $[TiO_2]$  or  $[3,4\text{-xylene}]$ ) indicate that the reaction follows saturation-type kinetics. The process kinetics are directly proportional to the light intensity ( $I$ ) at low light fluxes, scale with  $I^{1/2}$  at higher fluxes and are independent of  $I$  at very high fluxes ( $k \sim f(I^0)$ ). This result is consistent with expectations and accords with the experimental observations.

The major primary intermediates identified in the photodegradation of xylenols were either dihydroxydimethylbenzenes and/or dimethylbenzoquinones; other intermediates were also formed but were not identified. Elsewhere [26], we report recent pulse radiolytic studies on these xylenols to determine the initial radicals that are formed on attack by  $\cdot OH$  radicals, and which subsequently yield the observed intermediate products reported here (Table 1).

This work adds another example of a class of environmental organic contaminant that occurs in wastewaters and that can be degraded efficiently by photocatalytic methods.

#### Acknowledgements

This work was supported by the Natural Sciences and Engineering Research Council of Canada. We are also grateful to the North Atlantic Treaty Organization for a Collaborative Exchange Grant (No. CRG 089746) with Drs. Fox (TX), Pelizzetti (Torino) and Pichat (Lyon).

#### References

- [1] M.A. Callahan, M. Slimak, N. Gbel, I. May, C. Fowler, R. Freed, P. Jennings, R. Dupree, F. Whitemore, B. Maestri, B. Holt and C. Gould, *Water Related Environmental Fate of 120 Priority Pollutants, Report No. EPA-440/14-79-029a,b*, United States Environmental Protection Agency, NTIS, Washington DC, 1979.
- [2] J.G. Mueller, P.J. Chapman and P.H. Pritchard, *Environ. Sci. Technol.*, **23** (1989) 1197.
- [3] D.F. Goerlitz, D.E. Troutman, E.M. Godsy and B.J. Franks, *Environ. Sci. Technol.*, **19** (1985) 955, and references cited therein.
- [4] D. Bahnemann, J. Cunningham, M.A. Fox, E. Pelizzetti, P. Pichat and N. Serpone, in D. Crosby, G. Helz and R. Zepf (eds.), *Aquatic and Surface Photochemistry*, Lewis Publishers, Boca Raton, FL, 1994, pp. 261–316.
- [5] R. Terzian, N. Serpone, C. Minero and E. Pelizzetti, *J. Catal.*, **128** (1991) 352.
- [6] *Technical Bulletin No. 56*, Degussa Canada Ltd., 4261 Mainway Drive, Burlington, Ont., 1982.
- [7] *Oriel Corporation Catalog, Vol. III, Optics and Filters*, Stratford, CT, 1990.
- [8] (a) N. Serpone, E. Pelizzetti and H. Hidaka, in Z.W. Tian and Y. Cao (eds.), *Photochemical and Photoelectrochemical Conversion and Storage of Solar Energy*, International Academic Publishers, Beijing, China, 1993, pp. 33–73. (b) N. Serpone, R. Terzian, D. Lawless, P. Kennepohl and G. Sauve, *J. Photochem. Photobiol. A: Chem.*, **73** (1993) 11.
- [9] K.J. Laidler, *Chemical Kinetics*, Harper & Row, New York, 3rd edn., 1987.
- [10] E.P. Serjeant and B. Dempsey, *Ionization Constants of Organic Acids in Aqueous Solution, IUPAC Chemical Data Series No. 23*, Pergamon, Oxford, 1979.
- [11] M. Barbeni, E. Pramauro, E. Pelizzetti, E. Borgarello, M. Grätzel and N. Serpone, *Nouv. J. Chim.*, **8** (1984) 550.
- [12] M. Barbeni, E. Pelizzetti, E. Borgarello and N. Serpone, *Chemosphere*, **14** (1985) 195.
- [13] (a) K. Okamoto, Y. Yamamoto, H. Tanaka, M. Tanaka and A. Itaya, *Bull. Chem. Soc. Jpn.*, **58** (1985) 2015. (b) K. Okamoto, Y. Yamamoto, H. Tanaka and A. Itaya, *Bull. Chem. Soc. Jpn.*, **58** (1985) 2023.
- [14] K. Sehested, H. Corfitzen, H.C. Christensen and E.J. Hart, *J. Phys. Chem.*, **79** (1975) 310.
- [15] C.S. Turchi and D.F. Ollis, *J. Catal.*, **122** (1990) 178.
- [16] T.A. Egerton and C.J. King, *J. Oil Colour. Chem. Assoc.*, **62** (1979) 386.
- [17] M.W. Peterson, J.A. Turner and A.J. Nozik, *J. Phys. Chem.*, **95** (1991) 221.

- [18] D.F. Ollis, in E. Pelizzetti and M. Schiavello (eds.), *Photochemical Conversion and Storage of Solar Energy*, Kluwer Academic Publishers, Netherlands, 1991, p. 593.
- [19] J.C. D'Oliveira, G. Al-Sayyed and P. Pichat, *Environ. Sci. Technol.*, 24 (1990) 990.
- [20] (a) J.R. Bolton, *Proceedings First International Conference on Advanced Oxidation Technologies for Water and Air Purification, June 25–30, 1994, London, Ontario, Canada*. (b) J.E. Valladares and J.R. Bolton, in D.F. Ollis and H. Al-Ekabi (eds.), *Photocatalytic Purification and Treatment of Water and Air*, Elsevier, Amsterdam, 1993, pp. 111–120.
- [21] N. Serpone, D. Lawless and E. Pelizzetti, *J. Phys. Chem.*, submitted.
- [22] A. Scialfani, L. Palmisano and M. Schiavello, *J. Phys. Chem.*, 94 (1990) 829.
- [23] H. Hidaka, J. Zhao, S. Suenaga, E. Pelizzetti and N. Serpone, *J. Jpn. Oil Chem. Soc.*, 39 (1990) 45.
- [24] G. Al-Sayyed, J.C. D'Oliveira and P. Pichat, *J. Photochem. Photobiol. A: Chem.*, 58 (1991) 99.
- [25] G. Rothengerger, J. Moser, M. Gratzel, N. Serpone and D.K. Sharma, *J. Am. Chem. Soc.*, 107 (1985) 8054.
- [26] R. Terzian, N. Serpone and M.A. Fox, *J. Photochem. Photobiol. A: Chem.*, to be published (1995).